Progress In Electromagnetics Research, Vol. 137, 335–357, 2013

A NOVEL SPARSE STEPPED CHAOTIC SIGNAL AND ITS COMPRESSION BASED ON COMPRESSIVE SENSING

Jiefang Yang[1, 2, *] and Yunhua Zhang[1]

[1]The Key Laboratory of Microwave Remote Sensing, Chinese Academy of Sciences, Beijing 100190, China

[2]University of Chinese Academy of Sciences, Beijing 100049, China

Abstract—We propose a novel signal model by combining the sparse stepped frequency signals with chaotic signals, i.e., the sparse stepped chaotic signal (SSCS) model, as well as the corresponding compression algorithm based on compressed sensing. In SSCS, the chaotic signals are modulated to sparse stepped frequencies to compose a transmitting burst. When receiving, the echo signals are demodulated to the baseband and then can be sampled directly at a rate much lower than the Nyquist rate determined by the bandwidth of chaotic signal of each subpulse. Compared with radars using conventional stepped frequency waveforms, the SSCS radar can transmit fewer subpulses in a burst and directly use lower speed ADC next to the receiver. Both simulated and real radar data are processed to demonstrate the effectiveness of the proposed SSCS as well as the compression algorithm by which high resolution range profiles are very well reconstructed.

1. INTRODUCTION

High-resolution synthetic aperture radar (SAR) and inverse synthetic aperture radar (ISAR) have been widely applied in both civilian and military fields. In order to get high-resolution range profile, the stepped frequency chirp signal (SFCS) was proposed and applied practically. SFCS is composed of a burst of narrow-band subpulse chirp signals with their carrier frequencies increased/decreased linearly or nonlinearly [1–4]. It can be synthesized to get a wide band signal with subaperture processing [4]. In order to nullify grating

Received 1 December 2012, Accepted 19 February 2013, Scheduled 22 February 2013

* Corresponding author: Jiefang Yang (jfyang.xd@163.com).

lobes, the frequency step must be smaller than the bandwidth of each subpulse [2].

Random noise radar is a kind of radar which transmits stochastic/pseudo-stochastic signals [5–12]. It has good performance on electronic counter countermeasure (ECCM) and very low probability of interception, as well as achieving approximately "thumbtack" ambiguity function [5, 6]. Chaotic signal is one kind of pseudo-stochastic signals which has already been used in random noise radars [9–12]. In [10], point target imaging using chaotic FM signals was simulated. In [11], placeFlores analyzed a set of chaos-based FM signals for wideband radar imaging and assessed their resolution capability and sidelobe distribution on the range-Doppler plane.

The compressive sensing (CS) theory [13–16] states that, it is possible to reconstruct sparse or compressible signals from highly incomplete samples or measurements, which are even much fewer than what is required according to the Nyquist Theorem. As we know, the application of CS has two preconditions that: (1) the under reconstructed signal is sparse or compressible, (2) the measurements are incoherent. Since many SAR/ISAR images are sparse or compressible in some proper bases, the CS theory has shown very good prospects in SAR/ISAR applications [17–34].

The usually adopted stepped frequency signals for achieving high-resolution range profile have obvious drawbacks: (1) quite a few number of subpulses are needed in a burst and the echoes of each subpulse must be recorded, this will definitely lead to large amount of data and bring large pressure on data sampling and storage; (2) It is sensitive to the phase errors, only small phase errors among the subpulses can degrade the range profile seriously; (3) the frequency gaps between adjacent subpulses are not allowed, or it will generate grating lobes. There were some methods proposed to overcome these drawbacks. In [36], the authors applied super-SVA methods to fill the spectrum gaps between subchirps in SFCS model. However when the gaps are larger than the bandwidth of one subchirp, the method may fail. In [22–23], the authors proposed sparse stepped frequency chirp signal for ISAR imaging using CS theory. Although the amount of data and acquisition time can be reduced, the determinate waveform of subpulse chirp signal will lead to relatively complicated down-sampling scheme, and at the same time, this kind of signal is very weak to resist interference.

Up to now, most of the reported random noise radars use fixed carrier frequency which once transmit only one pulse. Since it is usually difficult to generate ultra-wide-band random signals in one pulse, so is it to obtain high range resolution. Although some works

on applying CS to random noise radar to reduce the data have been carried out [31–34], most of them just presented simulation results but not real experiment results.

In this paper, we propose the sparse stepped chaotic signal (SSCS) model for ultra wideband SAR imaging through combining the stepped frequency technology, compressive sensing and chaotic signal together. In this model, chaotic signals are modulated to sparsely stepped carrier frequencies. The echo signals are demodulated to the baseband and then sampled at a rate much lower than the Nyquist rate which is at least two times of the bandwidth of each chaotic subpulse (the "Nyquist rate" refers to hereafter in this paper). Since the transmitted waveform is chaotic, the echo data are incoherent inherently, thus it is very suitable for applying the CS theory and realizing downsampling directly. We also propose a novel compressing algorithm for SSCS to get high-resolution range profile based on both CS and subaperture algorithms [4, 13–16]. Both simulated data and real radar data of 4 GHz bandwidth from a moving train are processed to verify the proposed algorithm. Compared with the radars using conventional stepped frequency waveforms [1–4], the SSCS radar may transmit fewer subpulses in a burst and uses lower speed ADC next to the receiver, so the hardware design of the radar system can be simplified and the pressure of data sampling and storage can be alleviated. Due to the stochastic property of the chaotic signals, the SSCS radar has good characteristics of low probability of interception (LPI) and low probability of detection (LPD). Different from the sparse stepped frequency chirp signal used in [22, 23], the bandwidth of the chaotic signal of each subpulse is much larger, so we can synthesize a wideband with just fewer subpulses and the model has more advantages in anti-jamming. Compared with the Super-SVA technique used in [36], the CS approach we proposed is more robust, and the frequency gaps between subpulses can be larger than the bandwidth of one subpulse.

The organization of the paper is as follows. Section 2 reviews the CS theory briefly. In Section 3, the SSCS model is proposed. In Section 4, we describe the novel compressing algorithm for SSCS. The experiment results of simulation and real radar data are given in Section 5 to show the effectiveness of the proposed approach. The conclusion is drawn and the further works are addressed in Section 6.

2. OVERVIEW OF COMPRESSIVE SENSING

Suppose a discrete signal $\mathbf{x} \in \mathbf{C}^{N\times 1}$, which can be represented by an orthonormal basis $\mathbf{\Psi} \in \mathbf{C}^{N\times N}$:

$$\mathbf{x} = \mathbf{\Psi}\boldsymbol{\alpha} \tag{1}$$

When there are only $K \ll N$ nonzero (or far larger than zero) elements in $\boldsymbol{\alpha} \in \mathbf{C}^{N\times 1}$, we call $\mathbf{x}$ a K-sparse signal under the basis $\mathbf{\Psi}$.

We use a matrix $\mathbf{\Phi} \in \mathbf{C}^{M\times N}$ to represent the measurement process, the collected data $\mathbf{y} \in \mathbf{C}^{M\times 1}$ $(M < N)$ can be expressed as:

$$\mathbf{y} = \mathbf{\Phi}\mathbf{x} + \mathbf{n} \tag{2}$$

$\mathbf{n}$ is the additive noise in the measurement process.

By combine (1) and (2), we can get:

$$\mathbf{y} = \mathbf{\Phi}\mathbf{\Psi}\boldsymbol{\alpha} + \mathbf{n} = \mathbf{\Theta}\boldsymbol{\alpha} + \mathbf{n} \tag{3}$$

where $\mathbf{\Theta} = \mathbf{\Phi}\mathbf{\Psi} \in \mathbf{C}^{M\times N}$ is called the sensing matrix.

The reconstruction of $\mathbf{x}$ is equivalent to the reconstruction of $\boldsymbol{\alpha}$. According to the CS theory, when $\mathbf{\Theta}$ satisfy the restricted isometry property (RIP) [13], the signal $\boldsymbol{\alpha}$ can be recovered from $\mathbf{y}$ with overwhelming possibility by solving the following optimization problem:

$$\min \ ||\boldsymbol{\alpha}||_{l_1} \quad s.t. \quad ||\mathbf{\Theta}\boldsymbol{\alpha} - \mathbf{y}||_{l_2} \ \leq \ \varepsilon \tag{4}$$

where $||\bullet||_{l_1}$ denotes the l_1-norm, ε is an upper bound on the size of the noisy contribution and $||\mathbf{n}||_{l_2} \leq \varepsilon$.

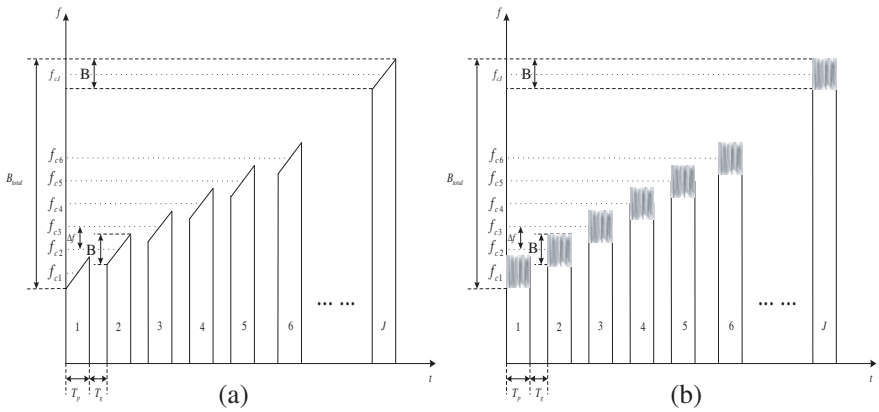

Figure 1. The conventional stepped frequency signal model. (a) Chirp signal as subpulse waveform; (b) chaotic signal as subpulse waveform. The subpulse number is J, the bandwidth of each subpulse is B, and the carrier frequency of j-th subpulse is $f_{cj} = f_c + (j-1)\cdot\Delta f$.

The RIP imposes that there exists a $\delta_K \in (0,\ 1)$ such that,

$$(1 - \delta_K)||\boldsymbol{\alpha}||_2 \leq ||\boldsymbol{\Theta}\boldsymbol{\alpha}||_2 \leq (1 + \delta_K)||\boldsymbol{\alpha}||_2 \tag{5}$$

holds for an arbitrary K-sparse vector $\boldsymbol{\alpha}$. The smallest δ_K is called the restricted isometry constant (RIC) of $\boldsymbol{\Theta}$. To recover the K-sparse vector $\boldsymbol{\alpha}$, δ_{2K} should be smaller than 1.

The RIP states that the mapping $\boldsymbol{\Theta}$ acts like an isometry mapping on an arbitrary K-sparse vector $\boldsymbol{\alpha}$. That is to say, an arbitrary subset of K columns taken from $\boldsymbol{\Theta}$ is nearly orthogonal.

There are many approaches can be used to reconstruct the K-sparse vector $\boldsymbol{\alpha}$ in Equation (4), such as l_1-minimization methods, greedy algorithms, iterative thresholding, and so on. In this paper, we choose the SPGL1 algorithm owning to its advantages in dealing with large-scale sparse reconstruction.

3. SPARSE STEPPED CHAOTIC SIGNAL (SSCS) MODEL

First, let's describe the conventional stepped frequency signal model as shown in Figure 1 briefly. Narrowband pulses of some waveforms are modulated on stepped carrier frequencies forming a burst as the radar's transmitting signal. The waveform of subpulse can be chirp or chaotic signal or other signal forms. Here we take chirp and chaotic signal as examples. Suppose there are J subpulses in a burst, and the bandwidth of each subpulse is B. The subpulses' carrier

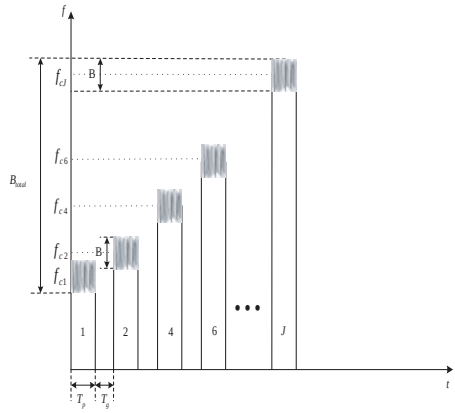

Figure 2. The sparse stepped chaotic signal (SSCS) model. It is constructed by randomly choosing M subpulses from the total J subpulses in Figure 1(b).

frequencies are $f_{cj} = f_c + (j-1) \cdot \Delta f$, in which f_c is the start frequency, Δf is the frequency step and must be smaller than B, $j = 1, 2, 3, \ldots J$. The total bandwidth of a burst after synthesization is $B_{total} = B + (J-1) \cdot \Delta f$. The echo signals of each subpulse are demodulated to baseband and then sampled at the Nyquist rate F_S. Then the subaperture algorithm in [4] can be used to reconstruct a high resolution range profile.

Now, we propose the sparse stepped chaotic signal (SSCS) model as shown in Figure 2. It is constructed by drawing M subpulses from the total J subpulses of chaotic signals randomly to form a transmitting burst, whose carrier frequencies are f_{cj_1}, f_{cj_2}, f_{cj_3}, $\ldots$ f_{cj_M}. At the same time we use chaotic signal for each subpulse. The echo signals are demodulated to baseband and then sampled at a rate much lower than the Nyquist rate F_S. The SSCS can be easily implemented into an existing radar system on the basis of conventional stepped frequency chirp signal.

4. CS-SUBAPERTURE ALGORITHM

In this section, we propose the CS-subaperture algorithm for compressing the SSCS based on both CS and subaperture algorithms [4, 13–16], as shown in Figure 3. The algorithm procedure is explained as follows.

Step1: Reconstruct the coarse range profile from the downsampled echo of each subpulse by using the CS algorithm.

In general, the echo signals $s_R(t)$ of a subpulse can be written as the convolution of the transmitted subpulse $s(t)$ with the target function $\sigma(t)$, which is described as:

$$s_R(t) = \int_{-\infty}^{\infty} s(t-\tau)\sigma(\tau)d\tau + \eta(t) \tag{6}$$

where $\eta(t)$ is the additive noise.

Suppose the echo signals are demodulated to baseband and sampled at the Nyquist rate F_S, then in the discrete domain, the echo data can be written as:

$$s_R\,[n] = \sum_{l=1}^{N_T} s[n-l] \cdot \sigma[l] + \eta[n] \tag{7}$$

where N_T is the sampling length of $s_R(t)$.

Let's use the vector $s_R \in \mathbf{C}^{N_T \times 1}$ to represent the sampled echo data, which can be formulated as:

$$s_R = \mathbf{A}\boldsymbol{\sigma} + \boldsymbol{\eta} \tag{8}$$

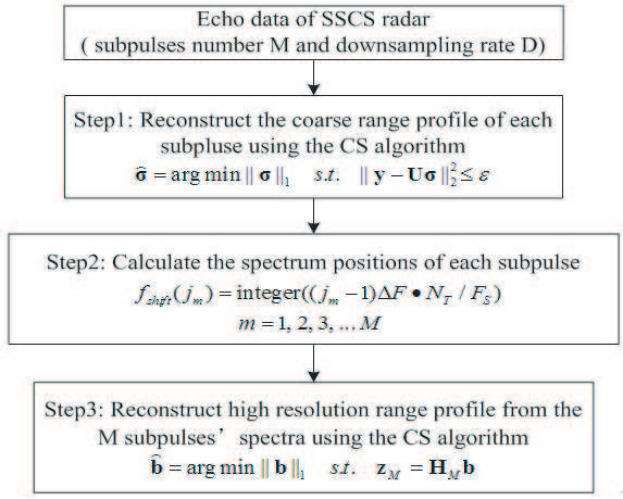

Figure 3. The flowchart of the CS-subaperture algorithm.

In the above equation, $\boldsymbol{\sigma} \in \mathbf{C}^{N_T \times 1}$ is the discrete range profile; $\boldsymbol{\eta} \in \mathbf{C}^{N_T \times 1}$ is the additive noise in the echo data; $\mathbf{A} \in \mathbf{C}^{N_T \times N_T}$ is the discrete convolution matrix constructed based on the complex baseband signal of transmitted subpulse $s(t)$. For the construction of $\mathbf{A}$ one can refer to [26, 27] and it will not be repeated here.

Suppose there are only K ($K \ll N_T$) scatterers in the range scene. That is to say, the number of nonzero elements in the vector σ is K [27]. Then, we can say that s_R has a sparse representation under $\mathbf{A}$, and $\mathbf{A}$ is the sparse matrix.

In SSCS radar, the echo signals are sampled at the rate of F_D, which is much lower than F_S. Let's use a vector $\mathbf{y} \in \mathbf{C}^{N_D \times 1}$ to represent the sampled echo signals, which can be obtained by uniformly downsampling the echo data s_R. This operation can be represented by a downsampling matrix $\mathbf{V}$, which is a partial unit matrix, and can be written as:

$$\mathbf{V}_{N_D \times N_T} = \{v_{n_d, n_t}\} = \begin{cases} 1, & n_t = D \cdot (n_d - 1) + 1 \\ 0, & \text{others} \end{cases}$$
$$n_d = 1, 2, \ldots N_D, \quad n_t = 1, 2, \ldots N_T. \tag{9}$$

where $D = \frac{F_S}{F_D}$ is called the downsampling rate.

Then, $\mathbf{y}$ can be represented as follows:

$$\mathbf{y} = \mathbf{V}s_R = \mathbf{V}(\mathbf{A}\boldsymbol{\sigma} + \boldsymbol{\eta}) = \mathbf{U}\boldsymbol{\sigma} + \mathbf{n} \tag{10}$$

In the above equation, $\mathbf{n} = \mathbf{V}\boldsymbol{\eta} \in \mathbf{C}^{N_D \times 1}$ is the noise in the echo data of SSCS radar; $\mathbf{U} = \mathbf{VA} \in \mathbf{C}^{N_D \times N_T}$ is the sensing matrix. $\mathbf{A}$ is the discrete convolution matrix constructed by the transmitted chaotic subpulse signal. Since the chaotic signal has very good incoherent property, the correlation between different columns in $\mathbf{A}$ is very low, i.e., $\mathbf{A}$ is an approximately orthogonal matrix. $\mathbf{U}$ is constructed by extracting the rows of $\mathbf{A}$ uniformly and the approximate orthogonality in columns can be held on, i.e., $\mathbf{U}$ is expected to meet RIP condition well. This will be verified further in Section 5.

According to the CS theory, we can reconstruct $\boldsymbol{\sigma}$ through solving the following equation:

$$\widehat{\boldsymbol{\sigma}} = \arg\min ||\boldsymbol{\sigma}||_1 \quad s.t. \quad ||\mathbf{y} - \mathbf{U}\boldsymbol{\sigma}||_2^2 \leq \varepsilon \tag{11}$$

where ε is the upper bound on the size of the noisy contribution, $||\mathbf{n}||_{l_2} \leq \varepsilon$. $\widehat{\boldsymbol{\sigma}}$ is the reconstructed coarse range profile for one subpulse.

We process the M subpulses' echoes as above respectively, so M coarse range profiles can be obtained.

Step2: Calculate the spectrum positions of M coarse profiles in the synthesized spectrum of much wider bandwidth.

Transform the coarse range profiles into frequency domain by FFT operation, i.e.,

$$\mathbf{g}_{j_m} = FFT\left[\widehat{\boldsymbol{\sigma}}_{j_m}\right] \tag{12}$$

where $\widehat{\boldsymbol{\sigma}}_{j_m} \in \mathbf{C}^{N_T \times 1}$ is the range profile reconstructed from the j_m-th subpulse, and $\mathbf{g}_{j_m} \in \mathbf{C}^{N_T \times 1}$ is the corresponding spectrum.

Calculate the relative shift of the spectrum of the j_m-th profile according to the following equation [4]:

$$f_{shift}(j_m) = \text{integer}((j_m - 1)\Delta f \cdot N_T / F_S) \quad m = 1,\ 2,\ \cdots M \tag{13}$$

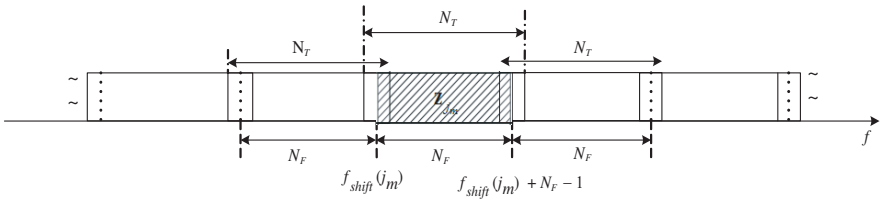

Figure 4. The schematic drawing of j_m-th subpulse's spectrum. The length of the spectrum is N_T, and the length of the effective part $\mathbf{z}_{j_m}$ is N_F. The indexes corresponding $\mathbf{z}_{j_m}$ in the synthesized spectrum are $f_{shift}(j_m) \sim f_{shift}(j_m) + N_F - 1$.

Since the bandwidth B of each subpulse is larger than the frequency step Δf, the spectra of any two adjacent subpulses will overlap. We should cut off the overlapped part and reserve the effective part of each spectrum in the synthesized spectrum. Let's use $\mathbf{z}_{j_m} \in \mathbf{C}^{N_F \times 1}$ to represent the effective part of the j_m-th subpulse's spectrum, which is the shadowed part in Figure 4 and $N_f = \text{integer}(\Delta f \cdot N_T/F_S)$. The indexes corresponding $\mathbf{z}_{j_m}$ in the synthesized spectrum are $f_{shift}(j_m) \sim f_{shift}(j_m) + N_F - 1$.

Step3: Reconstruct the high resolution range profile from the M subpulses' spectra utilizing the CS algorithm.

The length of the whole spectrum after synthesizing M subpulses is still approximately as $J \cdot N_F$ if we always keep the first and the last subpulses when randomly drawing. Let's use a vector $\mathbf{b} \in \mathbf{C}^{J \cdot N_F \times 1}$ to represent the high range profile. So the j_m-th subpulse's spectrum can be described as the following equation:

$$\mathbf{z}_{j_m} = \mathbf{H}_{j_m}\mathbf{b} \tag{14}$$

where $\mathbf{H}_{j_m}$ is a partial Fourier transform matrix, which can be structured as follow:

$$\mathbf{H}_{j_m} = \begin{bmatrix} 1 & W^{f_{shift}(j_m)} & \cdots & W^{f_{shift}(j_m)\cdot(J\cdot N_F-1)} \\ 1 & W^{f_{shift}(j_m)+1} & \cdots & W^{[f_{shift}(j_m)+1]\cdot(J\cdot N_F-1)} \\ \vdots & \vdots & \cdots & \vdots \\ 1 & W^{f_{shift}(j_m)+N_F-1} & \cdots & W^{[f_{shift}(j_m)+N_F-1]\cdot(J\cdot N_F-1)} \end{bmatrix}_{N_F \times J\cdot N_F} \tag{15}$$

In the above matrix, $W = e^{-j\frac{2\pi}{J\cdot N_F}}$.

After combing the M spectra, a new column vector can then be constructed:

$$\mathbf{z}_M = \begin{bmatrix} \mathbf{z}_{j_1} \\ \mathbf{z}_{j_2} \\ \vdots \\ \mathbf{z}_{j_M} \end{bmatrix}_{M\cdot N_F \times 1} \tag{16}$$

According to (14) and (16), we have following equations:

$$\mathbf{z}_M = \mathbf{H}_M\mathbf{b} \tag{17}$$

$$\mathbf{H}_M = \begin{bmatrix} \mathbf{H}_{j_1} \\ \mathbf{H}_{j_2} \\ \vdots \\ \mathbf{H}_{j_M} \end{bmatrix}_{M\cdot N_F \times J\cdot N_F} \tag{18}$$

where $\mathbf{H}_M$ is a random partial unit Fourier matrix, whose columns also satisfy the approximate orthogonality [23].

According to the CS theory, we can reconstruct $\mathbf{b}$ from the vector $\mathbf{z}_M$ by solving the following equation:

$$\widehat{\mathbf{b}} = \arg\min ||\mathbf{b}||_1 \quad s.t. \quad \mathbf{z}_M = \mathbf{H}_M \mathbf{b} \tag{19}$$

$\widehat{\mathbf{b}}$ is the finally reconstructed high resolution range profile.

5. EXPERIMENT

The experiment radar system works at Ku-band. It can transmit stepped frequency bursts with chirp or chaotic signal as the subpulse. The radar hardware system mainly consists of frequency synthesizer, transmitter, power amplifier, receiver, control electronics and data recording device. The major technical parameters of the system are listed in Table 1.

Table 1. Major technical parameters of the radar system.

Carrier frequency f_{cj}	Frequency step Δf	Subpulse bandwidth B	Subpulse width T_p
12.78 GHz–16.58 GHz	200 MHz	224 MHz	4 μs
Subpulse interval T_g	Subpulse number J	A/D sampling rate F_S	
2 μs	20	250 MHz	

According to the parameters in Table 1, the total bandwidth after synthesizing J subpulses is about $B_{total} = B + (J-1) \cdot \Delta f \approx 4\,\text{GHz}$, so the corresponding range resolution is about 0.0375 m.

We choose the improved Logistic-Map signal as the subpulse waveform. The discrete form of this chaotic function is expressed as:

$$x_{n+1} = f(x_n) = 1 - 2(x_n)^2 \quad x_n \in (-1, 1) \tag{20}$$

(20) is a nonlinear mapping function, which can be used to produce a pseudo-stochastic waveform given an arbitrary initial value. The detailed properties of the improved Logistic-Map signal can be found in [12]. Let the chaotic signal pass through a lowpass filter to generate a bandlimited baseband signal as the real part of the transmitted baseband waveform, and use the Hilbert transform to get the image part. Quadrature modulation is applied to get the IF signal, which is then up-converted to the final transmitted signal. The real part and the autocorrelation of the complex baseband chaotic signal are shown in Figure 5.

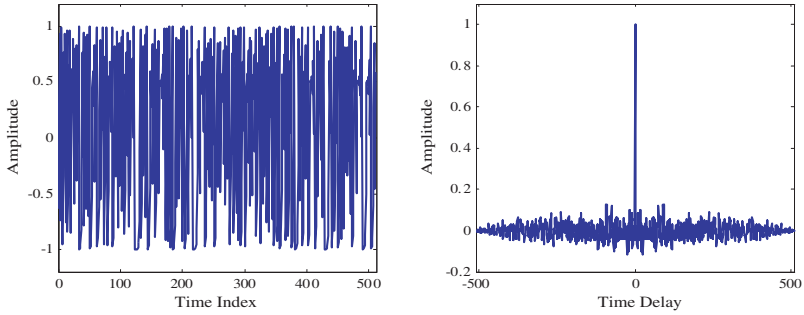

(a) (b)

Figure 5. The improved Logistic-Map signal: (a) the real part; (b) the autocorrelation.

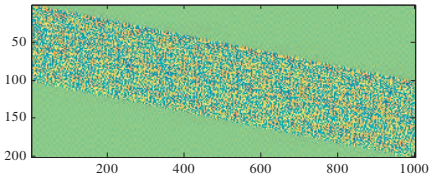

Figure 6. The real part of the sensing matrix constructed from the complex baseband Logistic-Map signal.

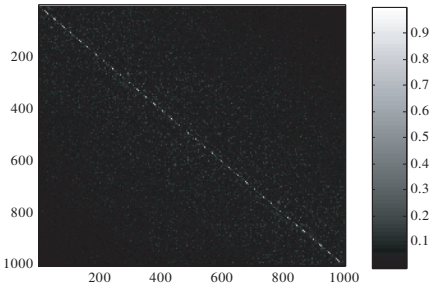

Figure 7. The column autocorrelation matrix. Each element is the scalar product of two columns in the sense matrix. Very good orthogonality is shown.

Taking downsampling rate $D = 5$ as an example, the real part of the sensing matrix constructed by the complex baseband chaotic signal is shown in Figure 6, which is mentioned in Equation (10). In this figure, the green color corresponds to zeros. It is clearly shown that the sensing matrix is a band matrix, and the nonzero elements are distributed following a band crossing the matrix from the upper left corner to the bottom right one. By calculating the scalar product of each column and the all columns in the matrix including itself, we can get the autocorrelation matrix, as shown in Figure 7, from which one can observe that the elements are mostly very small except those at the diagonal denoting the scalar product of a column itself. So the approximate orthogonality between different columns is verified, this means that the sensing matrix satisfy the RIP.

In the following, we will conduct simulations using SSCS with the parameters of Table 1 adopted. First, we evaluate the impulse response of CS-subaperture algorithm with SSCS. In the processing, we interpolate the results 10 times with zero-padding in frequency domain in order to show the main lobe and sidelobes clearly, though the impulse response of CS-subaperture algorithm looks like not "sparse". The results are shown in Figure 8. The results of one single 4 GHz bandwidth chaotic pulse and stepped frequency chaotic signal having 20 subpulses are represented for comparison, which are shown in Figures 8(a)–(b). There are grating lobes in the result of subaperture algorithm with SSCS having 10 subpulses, which are shown in Figure 8(c). Although super-SVA method can depress the grating lobes, the result is not perfect, which are shown in Figure 8(d). The result of CS-subaperture algorithm are shown in Figure 8(e), which are the same with the results of one single 4 GHz bandwidth chaotic pulse and stepped frequency chaotic signal having 20 subpulses.

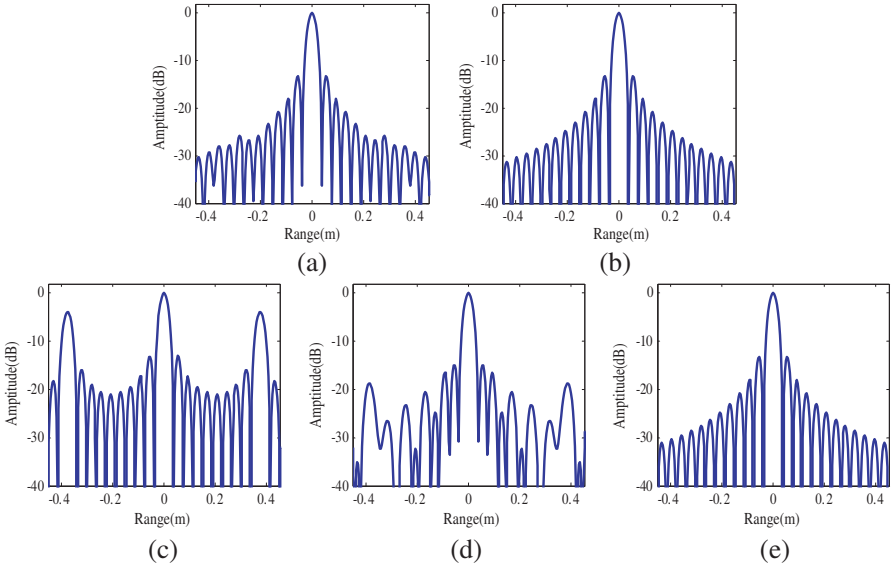

Figure 8. The impulse response diagrams. (a) Matched filter algorithm with single chaotic pulse of 4 GHz bandwidth; (b) subaperture algorithm with stepped frequency chaotic signal, subpulse number $M = 20$; (c) subaperture algorithm with SSCS, subpulse number $M = 10$; (d) subaperture algorithm with SSCS and super-SVA method filling the spectrum gaps, subpulse number $M = 10$; (e) CS-subaperture algorithm with SSCS, subpulse number $M = 10$, downsampling rate $D = 10$.

We use Monte Carlo method to evaluate our algorithm on Impulsion Response Width (IRW) and Peak Sidelobe Ratio (PSLR) [37] under different SNR. The results are shown in Figure 9. Each result is obtained by averaging the results of 100 runs. The IRW is consistent with the theoretical value 0.0375 m. The PSLR is consistent with the theoretical value 13.3 dB in high SNR environment (SNR $\geqslant$ 20 dB). In low SNR environment, when the downsampling rate D is large, the PSLR is a little lower than 13.3 dB.

Let us carry out one dimensional simulation with multiple targets. In order to be consistent with the real experiment, we set the interested scene to be 56–60 m far away from the radar. There are 7 targets in the scene, and the targets' true positions and amplitudes are listed in Table 2. The closest two targets are target 4 and target 5, which are separated by a distance of 0.07 m.

As for comparison reference, we represent the results of matched filter algorithm with one single chaotic signal of 4 GHz bandwidth and subaperture algorithm with stepped frequency chaotic signal having 20 subpulses, as shown in Figure 10. The result of subaperture algorithm without filling spectrum gaps and that of super-SVA method with the spectrum gaps filled are shown in Figure 11. The results of CS-subaperture algorithm are shown in Figure 12. All the results are

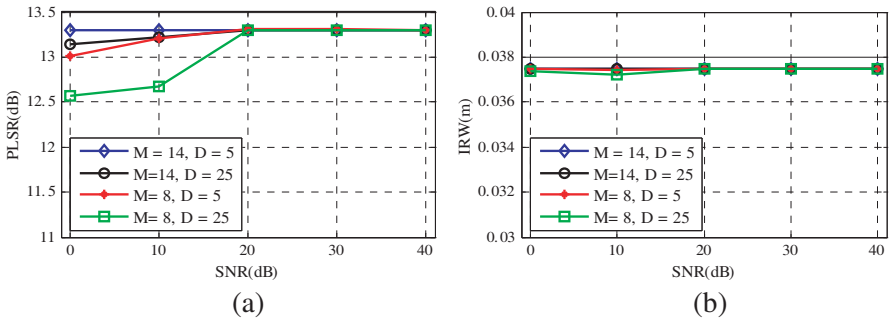

Figure 9. (a) PLSR versus SNR. (b) IRW versus SNR. The results are calculated with different subpulse number M and downsampling rate D.

Table 2. The target parameters (positions and amplitudes).

Target No.	1	2	3	4	5	6	7
Position (m)	56.5000	57.2500	57.6250	58.0000	58.0700	58.7500	59.5000
Amplitude	0.87	0.61	0.71	0.83	0.83	0.56	1.00

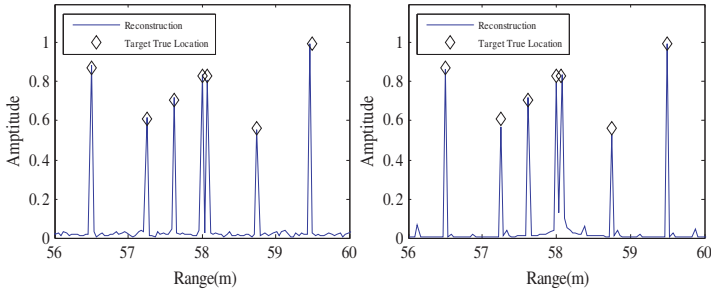

Figure 10. (a) The result of matched filter algorithm with one single chaotic pulse of 4 GHz bandwidth. (b) The result of subaperture algorithm with stepped frequency chaotic signal having 20 subpulses.

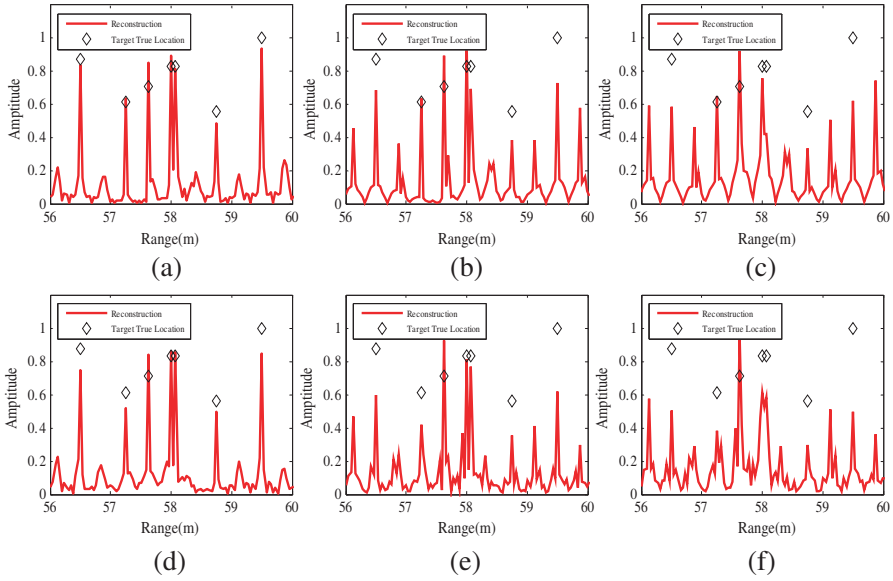

Figure 11. The result of subaperture algorithm with SSCS. (a), (b) and (c) are the results without filling the spectrum gaps, the corresponding subpulse number M are 16, 12, 8, respectively, while (d), (e), (f) are the results with spectrum gaps filled by super-SVA method, the corresponding subpulse number M are 16, 12, 8, respectively.

the original reconstructions without interpolation. From comparison of Figure 11 and Figure 12 we can see that, the range profiles reconstructed by subaperture algorithm are degraded seriously due

to the missing spectrum and the super-SVA method also fail in this situation, whereas the range profiles reconstructed by CS-subaperture algorithm with much less data are perfect.

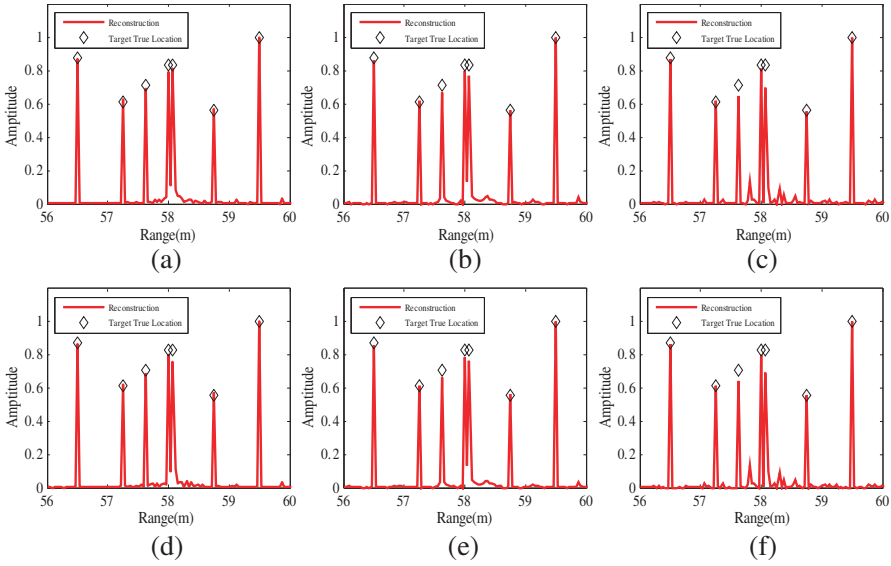

Figure 12. The results of CS-subaperture algorithm with SSCS with different subpulse number M and downsampling rate D. (a) $M = 16$, $D = 5$; (b) $M = 12$, $D = 5$; (c) $M = 8$, $D = 5$; (d) $M = 16$, $D = 10$; (e) $M = 12$, $D = 10$; (f) $M = 8$, $D = 10$.

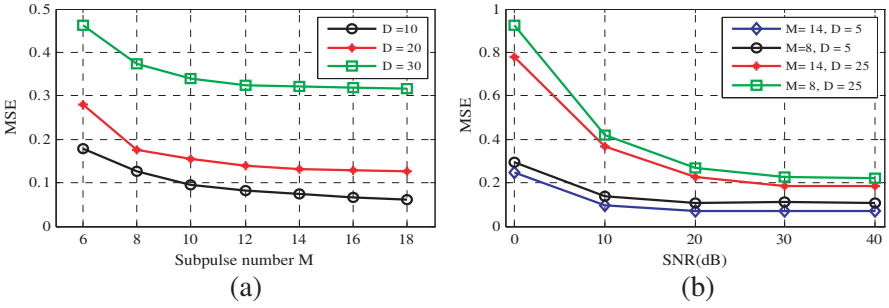

Figure 13. (a) The MSE versus subpulse number M. The results are calculated with different downsampling rate D in noise free environment; (b) the MSE versus SNR. The results are calculated with different subpulse number M and downsampling rate D.

Next, we use Monte Carlo method to evaluate our algorithm on the precision of targets reconstruction. The mean squared error (MSE) is taken as a performance measure, which is defined as follows:

$$MSE = \frac{\left\| \widehat{\mathbf{b}} - \mathbf{b} \right\|_2}{||\mathbf{b}||_2} \tag{21}$$

where $\widehat{\mathbf{b}}$ is the reconstructed range profile, and $\mathbf{b}$ is the truth. The MSEs of CS-subaperture algorithm with different subpulse number M and downsampling rate D in noise free environment are calculated and presented in Figure 13(a), the MSEs of CS-subaperture in different SNR are shown in Figure 13(b). Each result is obtained by averaging the results of 100 runs. From Figure 13(a) we can see that, the CS-subaperture algorithm works very well in noise free environment as expected. Figure 13(b) shows that, in high SNR environment (SNR $\geqslant$ 20 dB), the CS-subaperture algorithm can reconstruct the targets accurately enough. However, in low SNR environment, when the downsampling rate D is large, the performance of this algorithm degrades remarkably. A disadvantage of the CS method rest with that it is sensitive to the environment noise, this point needs further investigation.

In the above, the proposed signal model and the compressing algorithm have been tested by simulation. Now, let's further test them by real experiment. In the experiment, the Beijing No. 13 light railway train is taken as the imaging target. Figure 14 gives a photo of the train for reference. The train has six compartments, each compartment is about 19.2 m long and the total length is about 118 m; each compartment has four similar doors and three similar windows; there are ventilators on the top of each compartment at both ends. In order to catch the whole train, the photo was taken in a squint-view. In the experiment, the radar system worked in a side-view. The experiment geometry can refer to Figure 6(c) in [38].

Figure 14. The picture of No. 13 light railway train in Beijing. The ventilators of air-conditioners are marked in the picture.

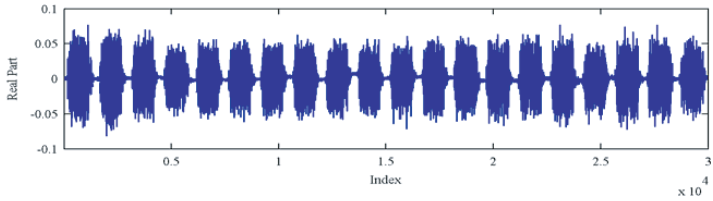

Figure 15. The baseband echoes of a burst of conventional stepped frequency chaotic signal. There are 20 subpulses in the burst. The sampling rate F_S is 250 MHz.

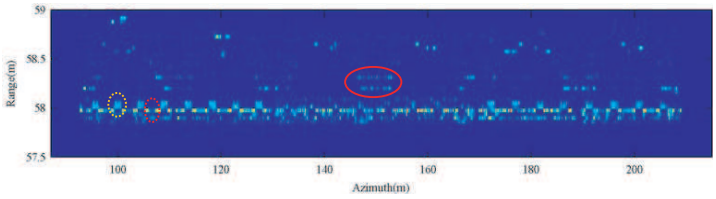

Figure 16. Imaging by subaperture algorithm with conventional stepped frequency chaotic signal (the all 20 subpulses are used). In the picture, ventilators are marked with a red solid circle, a door is marked with yellow dotted circle and a window is marked with red dotted circle.

In our experiment radar system, the transmitted burst consists of 20 subpulses. The echo signals are down-converted to baseband and sampled by the ADC at the rate of 250 MHz. The real parts of a burst of echoes are shown in Figure 15. There are 30,000 samples totally for a burst.

Range-Doppler (RD) algorithm is applied for imaging, and the subaperture algorithm is used to compress the echo signals in range, while the azimuthal compression can be referred to [35] and will not repeat here. The two-dimensional imaging result is presented in Figure 16. We should point out that due to the range profiles have not be calibrated, the range readings shown by the vertical axis are larger than the truth. In Figure 16, the six-compartment structure, doors, windows as well as ventilators are all clearly identified. In the image we marked ventilators with a red solid circle, a door with yellow dotted circle and a window with red dotted circle. One may notice that in the central two compartments, the "doors" and the "windows" are much blurred. An interesting explanation to this phenomenon is that there are much more passengers in the central compartments usually and this is the people lead to the much complicated scattering. We should illustrate that in order to clearly show the details, the vertical axis has

been exaggerated about 20 times compared with the horizontal axis.

In the observed scene, the train only occupies a few cells in range direction, thus, the scene is sparse in range direction. Now, let's select the echoes of some subpulses from the total 20 subpulses and perform downsampling operation on them so as to get the echo data of SSCS radar. Taking subpulse number 10 and downsampling rate 5 as an example, the real parts of the SSCS radar's echoes are shown in Figure 17. So there are just 3,000 samples totally.

The proposed CS-subaperture algorithm is used to compress the signals in range and traditional algorithm is used for azimuthal compression as mentioned above. The imaging results with different subpulse number M and downsampling rate D are presented in Figure 18 with (a), (b) and (c) respectively showing the results corresponding to $M = 16$, $D = 5$; $M = 14$, $D = 5$ and $M = 10$, $D = 5$. By comparing Figures 18 (a)–(c) with Figure 16, it is clearly shown that they all agree with each other very well, especially for the imaged structures of ventilators, doors, and windows.

One may ask such a question "why CS reconstruction algorithm is still workable with SSCS, although the whole signal spectrum is not continuous?" As we know, usually grating lobes are unavoidable in this case [2]. Our explanation is that: (1) the measurement matrix is formed through random selection of the signals along range direction; (2) the gaps just occupy a small part of the whole spectrum, so the absence of spectrum does not affect the random characteristics; (3) the signal is reconstructed through optimization process.

One may ask another question "With how less number of subpulses and with how less samples we still can reconstruct the range profiles?" This question is very difficult to answer because they are target dependent. This will be further investigated in the future. Here we can only point out a principle should be adhered to: we should keep the first and the last subpulses not skipped.

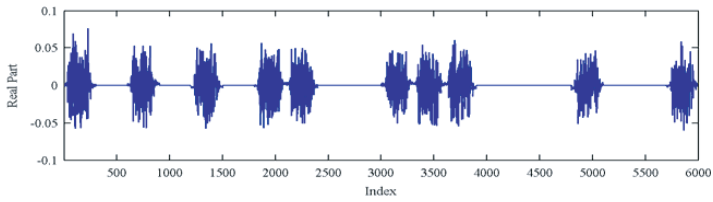

Figure 17. The baseband echoes of a burst of the SSCS. The 10 subpulses are choosen from the original total 20 subpulses. The downsampling rate $D = 5$, thus the corresponding sampling rate F in SSCS radar is 50 MHz.

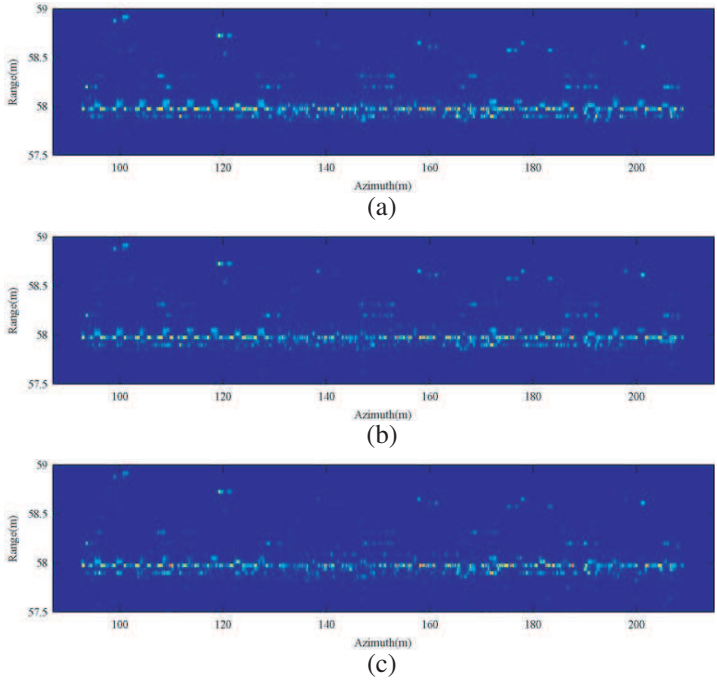

Figure 18. Imaging by CS-subaperture algorithm using SSCS with different subpulse number M and downsampling rate D. (a) $M = 16$, $D = 5$; (b) $M = 14$, $D = 5$; (c) $M = 10$, $D = 5$.

6. CONCLUSION

In this paper, we propose a sparse stepped chaotic signal (SSCS) model, as well as a novel compressing algorithm to get high-resolution range profile based on both CS and subaperture algorithms. By using SSCS, we can achieve the same resolution with much less data than that by using conventional stepped frequency signals. So the pressure of data sampling and storage for high-resolution radars can be alleviated. Both simulation and real experiment data are processed to verify the proposed signal model and the algorithm. However our work is far from end, there are many works deserve to be done in the future. Some of them are:

(1) At represent, the CS-subaperture algorithm is just suitable for targets with low radial velocity. The phase distortions caused by the velocity in subpulses are small and can be ignored in the processing. However, for moving targets with high radial velocity,

the distortions caused by the velocity can be large, which will degrade the range profile seriously, i.e., the motion compensation is inevitable. In most situations, the moving targets are sparse on the range-velocity plane, using CS theory to estimate the velocity of the targets and reconstruct the high-resolution range profile is a topic we are researching on.

(2) In the current experiment, the echo of SSCS radar is extracted from the existing echo data which is sampled according to the Nyquist sampling rate. In the future, we will construct the SSCS radar veritably by modifying our existing radar system;

(3) In this paper, we assume that the targets are point-like reflectors at discrete spatial positions, and the number of targets is much less than the total number of discrete spatial positions. Complex objects are approximately equal to a combination of independent point reflectors at discrete spatial positions. However, this model may not be suitable for all complex targets, so we should search other bases in which the specific complex targets can be sparsely expressed;

(4) We just use the improved Logistic-Map signal as the subpulse right now. In the future, we need to search other chaotic signals which may be more suitable for the sparse optimization reconstruction, that is to say, the sensing matrix constructed according to the signal should be much easier to satisfy the RIP.

REFERENCES

1. Levanon, N., "Stepped-frequency pulse-train radar signal," *IEE Proc-Radar Sonar Navigation*, Vol. 149, No. 6, 297–309, 2002.
2. Levanon, N. and E. Mozeson, "Nullifying ACF grating lobes in stepped-frequency train of LFM pulses," *IEEE Transactions on Aerospace and Electronic Systems*, Vol. 39, No. 2, 694–703, 2003.
3. Zhang, Q. and Y.-Q. Jin, "Aspects of radar imaging using frequency-stepped chirp signals," *Eurasip Journal on Applied Signal Processing*, Vol. 2006, No. 13, 1–8, 2006.
4. Zhang, Y. H., H. B. Li, and J. Wu, "Subaperture processing method for stepped frequency chirp signal," *Aerospace Electronics Information Engineering and Control*, Vol. 28, No. 1, 1–6, 2006.
5. Liu, G. S., H. Gu, X. H. Zhu, and W. M. Su, "The present and the future of random signal radars," *IEEE Aerospace and Electronic Systems Magazine*, Vol. 12, No. 10, 35–40, 1997.
6. Lukin, K. A. and R. M. Narayanan, "Fifty years of noise radar," *Seventh International Kharkov Symposium on Physics and*

Engineering of Microwaves, Millimeter and Submillimeter Waves, 1–3, 2010.

7. Narayanan, R. M., Y. Xu, P. D. Hoffmeyer, and J. O. Curtis, "Design, performance, and applications of a coherent ultra-wideband random noise radar," *Optical Engineering*, Vol. 37, No. 6, 1855–1869, 1998.
8. Narayanan, R. M., "Through-wall radar imaging using uwb noise waveforms," *Journal of the Franklin Institute-Engineering and Applied Mathematics*, Vol. 345, No. 6, 659–678, 2008.
9. Ashtari, A., G. Thomas, H. Garces, B. C. Flores, et al., "Radar signal design using chaotic signals," *2007 International Waveform Diversity & Design Conference*, 353–357, 2007.
10. Ding, K. and R. Yang, "Point target imaging simulation using chaotic signals," *2005 IEEE International Radar Conference Record*, 847–850, 2005.
11. Flores, B. C., E. A. Solis, and G. Thomas, "Assessment of chaos-based FM signals for range-doppler imaging," *IEE Proceedings-Radar Sonar and Navigation*, Vol. 150, No. 4, 313–322, 2003.
12. Wang, H. and J. D. Hu, "The improved logistic-map chaotic spread spectrum sequences," *Journal of China Institute of Communications*, Vol. 18, No. 8, 71–77, 1997.
13. Candes, E. J. and M. B. Wakin, "An introduction to compressive sampling," *IEEE Signal Processing Magazine*, Vol. 25, No. 2, 21–30, 2008.
14. Candes, E. J., J. Romberg, and T. Tao, "Robust uncertainty principles: Exact signal reconstruction from highly incomplete frequency information," *IEEE Transactions on Information Theory*, Vol. 52, No. 2, 489–509, 2006.
15. Candes, E. J. and T. Tao, "Near-optimal signal recovery from random projections: Universal encoding strategies?," *IEEE Transactions on Information Theory*, Vol. 52, No. 12, 5406–5425, 2006.
16. Donoho, D. L., "Compressed sensing," *IEEE Transactions on Information Theory*, Vol. 52, No. 4, 1289–1306, 2006.
17. Baraniuk, R. and P. Steeghs, "Compressive radar imaging," *2007 IEEE Radar Conference*, 128–133, 2007.
18. Herman, M. A. and T. Strohmer, "High-resolution radar via compressed sensing," *IEEE Transactions on Signal Processing*, Vol. 57, No. 6, 2275–2284, 2009.
19. Ender, J. H. G., "On compressive sensing applied to radar," *Signal Processing*, Vol. 90, 1402–1414, 2010.

20. Wei, S. J., X. L. Zhang, J. Shi, and G. Xiang, "Sparse reconstruction for SAR imaging based on compressed sensing," *Progress In Electromagnetics Research*, Vol. 109, 63–81, 2010.
21. Wei, S. J., X. L. Zhang, and J. Shi, "Linear array SAR imaging via compressed sensing," *Progress In Electromagnetics Research*, Vol. 117, 299–319, 2011.
22. Zhang, L., Z. J. Qiao, and M. D. Xing, "High-resolution ISAR imaging with sparse stepped-frequency waveforms," *IEEE Transactions on Geoscience and Remote Sensing*, Vol. 49, No. 11, 4630–4651, 2011.
23. Zhu, F., Q. Zhang, Q. Lei, and Y. Luo, "Reconstruction of moving target's HRRP using sparse frequency-stepped chirp signal," *IEEE Sensors Journal*, Vol. 11, No. 10, 2327–2334, 2011.
24. Yu, L. J. and Y. H. Zhang, "Random step frequency CSAR imaging based on compressive sensing," *Progress In Electromagnetics Research C*, Vol. 32, 81–94, 2012.
25. Zhang, L., Z. J. Qiao, M. D. Xing, J. L. Sheng, et al., "High-resolution ISAR imaging by exploiting sparse apertures," *IEEE Transactions on Antennas and Propagation*, Vol. 60, No. 2, 997–1008, 2012.
26. Alonso, M. T., P. Lopez-Dekker, and J. J. Mallorqui, "A novel strategy for radar imaging based on compressive sensing," *IEEE Transactions on Geoscience and Remote Sensing*, Vol. 48, No. 12, 4285–4295, 2010.
27. Xie, X. C. and Y. H. Zhang, "2D radar imaging scheme based on compressive sensing technique," *Journal of Electronics & Information Technology*, Vol. 32, No. 5, 1234–1238, 2010.
28. Chen, X. W., Y. H. Zhang, and X. K. Zhang, "FPGA based realization of AIC for applying CS to radar," *Progress In Electromagnetics Research C*, Vol. 19, 207–222, 2011.
29. Li, J., S. S. Zhang, and J. F. Chang, "Applications of compressed sensing for multiple transmitters multiple azimuth beams SAR imaging," *Progress In Electromagnetics Research*, Vol. 127, 259–275, 2012.
30. Liu, Z., X. Z. Wei, and X. Li, "Adaptive clutter suppression for airborne random pulse repetition interval radar based on compressed sensing," *Progress In Electromagnetics Research*, Vol. 128, 291–311, 2012.
31. Jiang, H., Y. Lin, B. Zhang, and H. Wen, "Random noise imaging radar based on compressed sensing," *Journal of Electronics & Information Technology*, Vol. 33, No. 2, 418–423, 2011.

32. Shastry, M. C., R. M. Narayanan, and M. Rangaswamy, "Compressive radar imaging using white stochastic waveforms," *2010 5th International Waveform Diversity and Design Conference*, 000090–000094, 2010.
33. He, Y. P., K. R. Wang, J. D. Zhang, and X. H. Zhu, "Compressive sensing based pseudo-random multi-phase CW radar," *Journal of Electronics & Information Technology*, Vol. 33, No. 3, 418–423, 2011.
34. Zhu, F., Q. Zhang, W. Hong, and F. F. Gu, "Sparse imaging method with strip-map random noise radar based on compressive sensing," *Systems Engineering & Electronics*, Vol. 34, No. 1, 56–63, 2012.
35. Bao, Z., M. D. Xing, and T. Wang, *Radar Imaging Technology,* Publishing House of Electronics Industry, Beijing, 2005.
36. Zhai, W. S. and Y. H. Zhang, "Application of super-SVA to stepped-chirp radar imaging with frequency band gaps between subchirps," *Progress In Electromagnetics Research B*, Vol. 30, 71–82, 2011.
37. Cumming, I and F. Wong, *Digital Processing of Synthetic Aperture Radar Data: Algorithms and Implementation,* Artech House, Boston, MA, 2005.
38. Zhang, X. K. and Y. H. Zhang, "High resolution moving train imaging experiments with stepped-frequency radar system," *2010 8th European Conference on Synthetic Aperture Radar,* 1–4, 2010.